CANCER

Epigenetic activation of the drug transporter OCT2 sensitizes renal cell carcinoma to oxaliplatin

Yanqing Liu,[1]* Xiaoli Zheng,[1]* Qinqin Yu,[1] Hua Wang,[2] Fuqing Tan,[3] Qianying Zhu,[1] Lingmin Yuan,[1] Huidi Jiang,[1] Lushan Yu,[1†‡] Su Zeng[1†‡]

Renal cell carcinoma (RCC) is known for its multidrug resistance. Using data obtained from the cancer transcriptome database Oncomine and the proteome database The Human Protein Atlas, we identified the repression of organic cation transporter OCT2 as a potential factor contributing to oxaliplatin resistance in RCC. By analyzing OCT2 expression in collected patient tissues and commercial tissue microarray specimens, we demonstrated OCT2 repression in RCC at both transcription and protein levels. Epigenetic analysis revealed that the repressed *OCT2* promoter in RCC is characterized by hypermethylated CpG islands and the absence of H3K4 methylation. Further mechanistic studies showed that DNA hypermethylation blocked MYC activation of *OCT2* by disrupting its interaction with the E-Box motif, which prevented MYC from recruiting MLL1 to catalyze H3K4me3 at the *OCT2* promoter and resulted in repressed *OCT2* transcription. Targeting this mechanism, we designed a sequential combination therapy and demonstrated that epigenetic activation of OCT2 by decitabine sensitizes RCC cells to oxaliplatin both in vitro and in xenografts. Our study highlights the potential of translating "omics" data into the development of targeted therapies.

INTRODUCTION

Renal cell carcinoma (RCC) is the most common form of kidney cancer and accounts for 2 to 3% of all cancers in adults (*1*). Prognosis of advanced RCC is extremely poor because of treatment resistance (*2*). Oxaliplatin is a platinum-based chemotherapy and is typically used in combination therapies for the treatment of colorectal cancer. Early clinical trials showed that oxaliplatin is ineffective against advanced RCC (*3*, *4*). One of the major mechanisms of platinum resistance in this cancer type is inadequate amounts of platinum reaching the target DNA (*5*). In vitro studies have shown that organic cation transporter 2 (OCT2; also known as SLC22A2) is the major transporter that enhances the cellular uptake and, consequently, cytotoxicity of oxaliplatin (*6*–*9*). A recent clinical study also showed that OCT2 expression correlates with prognosis of oxaliplatin-based chemotherapy in metastatic colorectal cancer patients (*9*). RCC originates from renal proximal tubules, where OCT2 is highly expressed (*10*). Our preliminary data mining revealed that OCT2 is repressed in RCC (*11*, *12*). The above evidence suggested a potential link between OCT2 repression and oxaliplatin resistance in RCC. Genes involved in platinum inactivation (*GSTP1*, *ABCC2*, *ATP7A*, *ATP7B*, and *MT1A*) and DNA repair deficiency (*ERCC1* and *ERCC2*) may co-contribute to oxaliplatin resistance (*5*, *13*–*15*). However, none of these genes shows consistent differences at the mRNA and protein levels between normal kidney and RCC (*11*, *12*), indicating that these genes do not contribute to oxaliplatin resistance in RCC.

Accumulating studies support an association of epigenetic changes in drug transporter genes with drug response in cancer (*16*, *17*). Epigenetic events are heritable changes in gene expression that are not mediated by alterations of the underlying DNA sequence, including DNA methylation, histone modifications, nucleosome remodeling, and noncoding RNA expression. Given the reversible nature of epigenetic alterations, combining epigenetic drugs with conventional chemotherapies has emerged as a promising treatment option to improve therapeutic efficacy in cancer treatment (*18*). Promoter DNA methylation controls the specific expression of OCT2 in human renal proximal tubules (*19*). However, whether and how epigenetic pathways are involved in OCT2 repression in RCC have been unclear.

Here, we determined the epigenetic mechanisms underlying OCT2 repression in RCC. We then designed a combination therapy to reactivate OCT2 expression and sensitize RCC cells to oxaliplatin.

RESULTS

OCT2 is repressed in RCC

Immunohistochemistry data from The Human Protein Atlas (HPA) demonstrated strong staining of OCT2 in normal kidneys and no staining in most of the RCC tissues using two antibodies targeting different epitopes of the OCT2 protein (fig. S1). To confirm this result, we analyzed OCT2 expression on an RCC tissue microarray (TMA). Consistent with data from HPA, OCT2 staining was positive in 24 of 31 samples from adjacent nontumor tissues but negative in all 31 RCC tumor tissue samples (Fig. 1, A and B). These results imply that OCT2 expression is repressed in RCC. Microarray data from Oncomine showed that *OCT2* transcription was down-regulated in RCC tissues compared with that in normal kidney (Fig. 1C) (*11*). To confirm this result, we profiled mRNA expression of *OCT2* in 46 pairs of RCC tumors and adjacent normal tissues. Consistent with high-throughput sequencing data, our quantitative polymerase chain reaction (qPCR) analysis confirmed that *OCT2* mRNA expression was significantly decreased in RCC tumor tissues compared with that in adjacent normal controls ($P < 0.0001$; Fig. 1D). These data together demonstrate that OCT2 is repressed at both mRNA and protein expression levels in RCC.

[1]Institute of Drug Metabolism and Pharmaceutical Analysis, Zhejiang Province Key Laboratory of Anti-Cancer Drug Research, College of Pharmaceutical Sciences, Zhejiang University, Hangzhou 310058, China. [2]Department of Urology, Cancer Hospital of Zhejiang Province, Hangzhou 310022, China. [3]Department of Urology, The First Affiliated Hospital, School of Medicine, Zhejiang University, Hangzhou 310003, China.
*These authors contributed equally to this work.
†Present address: College of Pharmaceutical Sciences, Zhejiang University, 866 Yuhangtang Road, Hangzhou 310058, China.
‡Corresponding author. Email: zengsu@zju.edu.cn (S.Z.); yuls@zju.edu.cn (L.Y.)

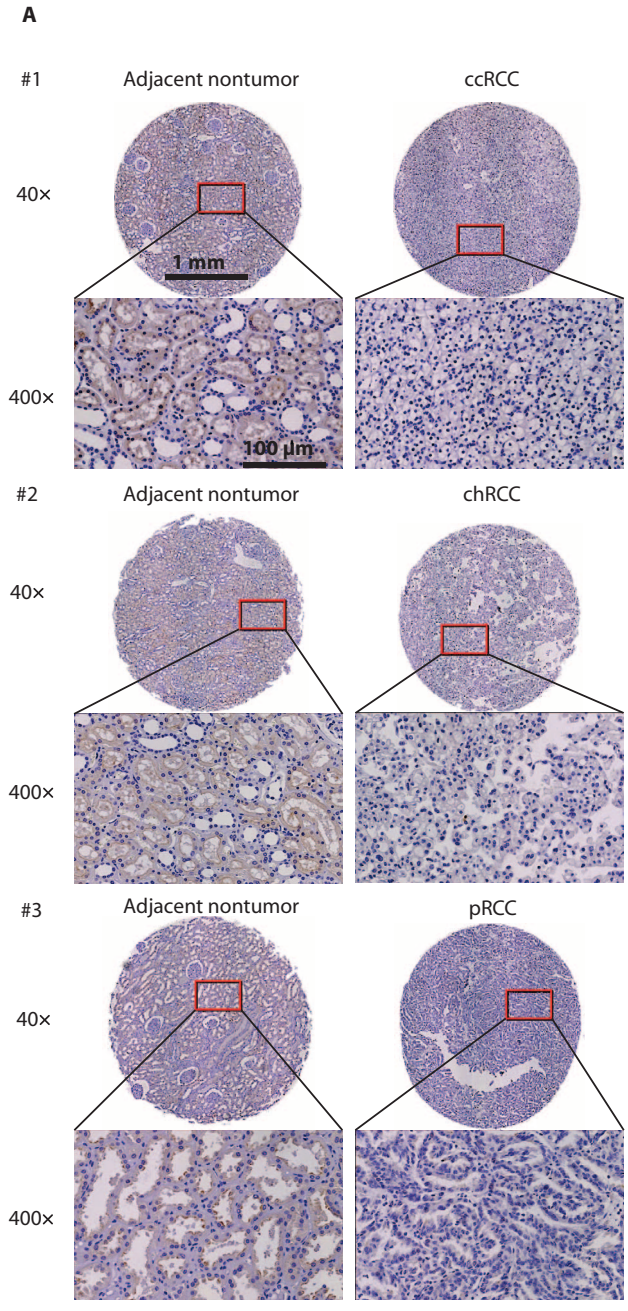

B

	Tumor (positive/total)	Adjacent nontumor (positive/total)	*P* value
ccRCC (*n* = 10)	0/10	6/10	
chRCC (*n* = 10)	0/10	9/10	
pRCC (*n* = 11)	0/11	9/11	
Total (*n* = 31)	0/31	24/31	<0.0001

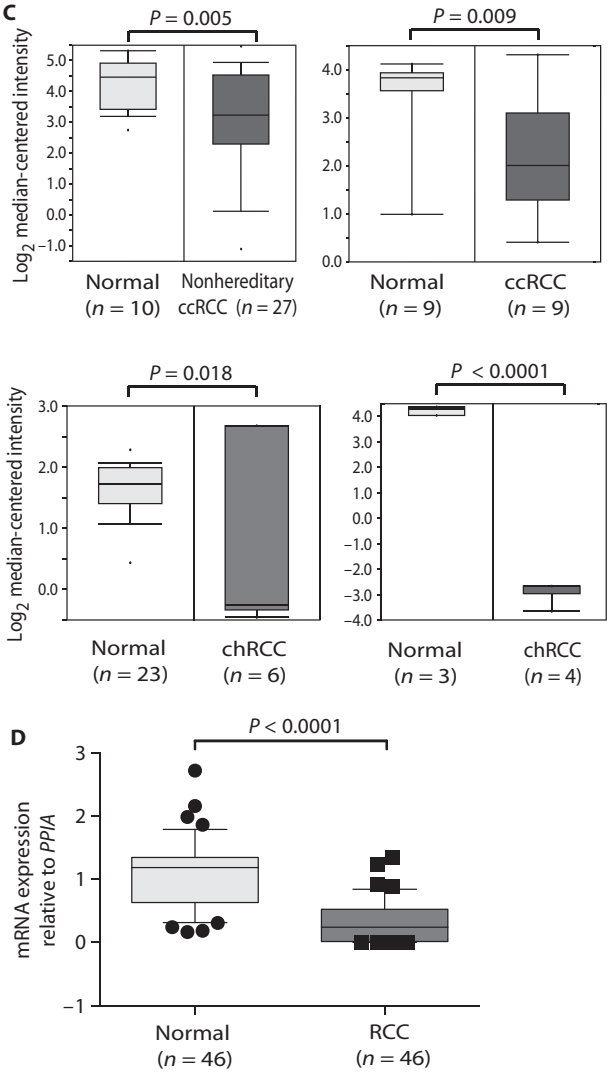

Fig. 1. OCT2 is repressed in RCC. (**A**) Representative images of immunohistochemistry staining for OCT2 protein on a TMA constructed from 31 pairs of RCC and adjacent nontumor tissue. ccRCC, clear cell RCC; chRCC, chromophobe RCC; pRCC, papillary RCC. (**B**) Statistical analysis of immunohistochemistry staining results for OCT2 from the TMA slide (two-tailed Fisher's exact test). (**C**) Meta-analysis of *OCT2* transcription using data sets from the Oncomine database (one-tailed unpaired *t* test). Data sets from four study groups (*48*–*51*) consistently show reduced *OCT2* transcription in RCC tissues compared with that in the normal kidney. The *y* axis represents $\log_2$ median-centered intensity (normalized expression). (**D**) qPCR analysis of *OCT2* transcription in RCC (two-tailed paired *t* test). RNA extracted from 46 pairs of RCC and adjacent nontumor tissue samples was used. For (C) and (D), shaded boxes represent the interquartile range (25th to 75th percentile). Whiskers represent the 10th to 90th percentile. The bars denote the median.

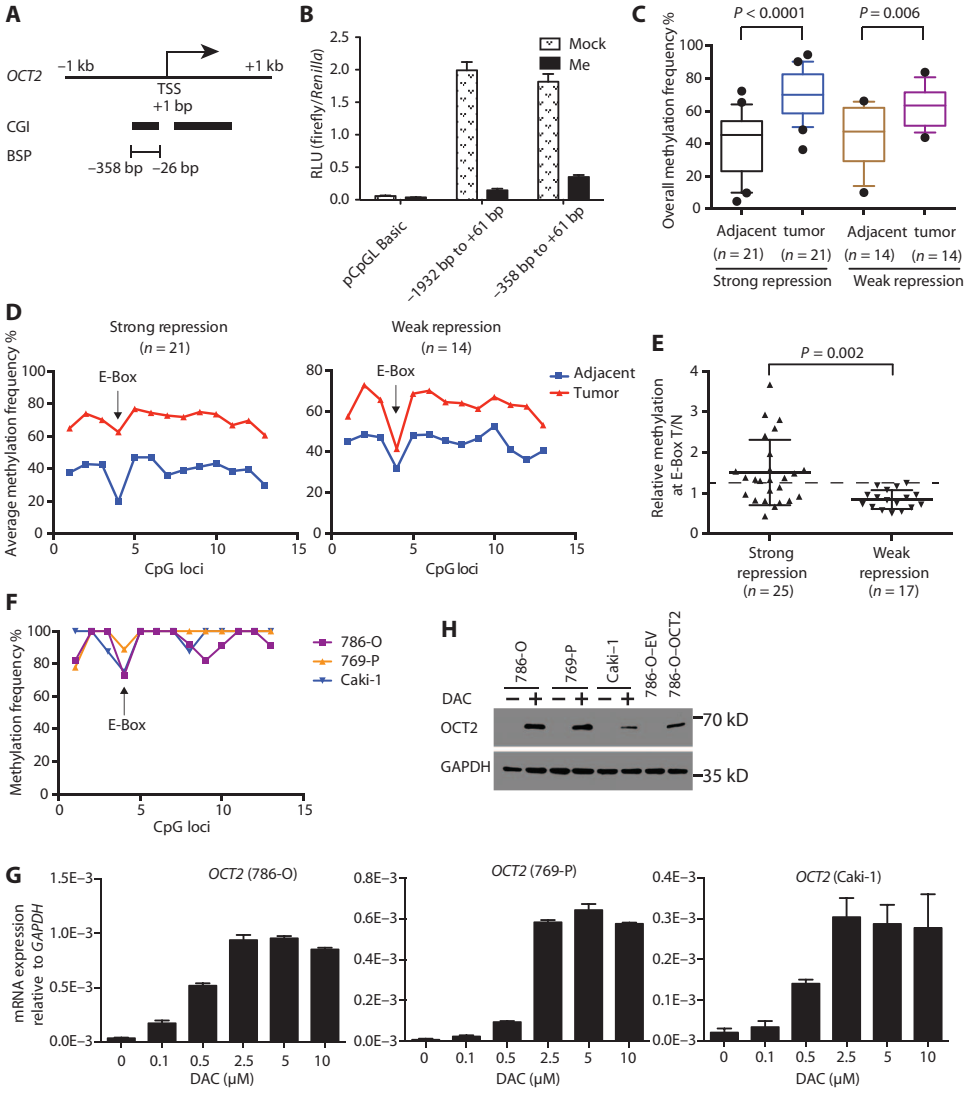

Fig. 2. DNA hypermethylation represses *OCT2* in RCC. (**A**) Schematic of the *OCT2* promoter region around transcription start site (TSS). (**B**) Luciferase assay in HEK293 cells. Promoter constructs were treated with (Me) or without (Mock) M.SssI. The *y* axis indicates relative light units (RLU). GAPDH, glyceraldehyde-3-phosphate dehydrogenase. (**C** and **D**) BSP analysis of *OCT2* CGI in RCC and matched adjacent nontumor tissues. Samples belong to the 46 pairs of tissues in Fig. 1D. Transcription reduced by at least 70% was considered strong repression (the alternative was weak repression). The *y* axis in (C) indicates the overall methylation percentage calculated from the 13 CpG loci in the sequenced region (two-tailed paired *t* test). Boxes represent the interquartile range (25th to 75th percentile). Whiskers represent the 10th to 90th percentile. The bars denote the median. The *y* axis in (D) indicates the average methylation percentage of each CpG site calculated from patient tissues with either OCT2 strong repression (left) or weak repression (right). (**E**) MS-AP-qPCR shows E-Box methylation status at the *OCT2* promoter in vivo (two-tailed unpaired *t* test). The *y* axis indicates E-Box percentage methylation ratio in tumors (T) and paired adjacent nontumor tissues (N). Methylation ratio T/N = 1.3 (indicated as the dashed line) is the threshold for hypermethylation (*21*). BSP and MS-AP-qPCR data from individual samples are provided in table S5. (**F**) BSP analysis of *OCT2* CGI in RCC cell lines. (**G**) RCC cell lines were treated by DAC at the indicated dosage for 72 hours. (**H**) RCC cell lines were treated with 2.5 μM DAC for 72 hours. Lysates from 786-O stably expressing *OCT2* complementary DNA (786-O–*OCT2*) or parent vector (786-O–EV) were loaded as control. Data are means ± SEM from biological triplicates in (B) and biological triplicates with technical duplicates in (G).

DNA hypermethylation represses OCT2 in RCC

Next, we attempted to identify the mechanisms that underlie *OCT2* repression in RCC. As shown in Fig. 2A, *OCT2* proximal promoter region contains two putative CpG islands (CGIs). To determine whether the *OCT2* promoter activity is controlled by DNA methylation, we performed a luciferase assay in human embryonic kidney (HEK) 293 cells. Two *OCT2* promoter fragments, −1932 base pairs (bp) to +61 bp and −358 bp to +61 bp, were cloned into the CpG-free luciferase reporter vector pCpGL Basic (*20*). After in vitro methylation by M.SssI methylase in the presence of *S*-adenosyl-L-methionine, transcriptional activity of both promoter constructs was inhibited by at least 80% (Fig. 2B), suggesting that DNA methylation directly represses the *OCT2* promoter activity in vitro. The upstream CGI at the *OCT2* promoter region −320 bp to −66 bp contains 13 CpG sites. DNA hypomethylation at this region regulates kidney-specific expression of OCT2 (*19*). To investigate whether aberrant DNA methylation regulates OCT2 repression in RCC, we used bisulfite sequencing PCR (BSP) to examine methylation at the upstream CGI of *OCT2*. We optimized the PCR using combined bisulfite restriction analysis to rule out unbiased amplification (fig. S2, A and B). Thirty-five pairs of RCC and matched adjacent nontumor tissues were used in the analysis. Compared with nontumor tissues, the overall methylation percentage in the sequenced region significantly increased in RCC tissues with both strong repression (transcription reduced by at least 70%; $P < 0.0001$) and weak repression of OCT2 (transcription reduced by less than 70%; $P = 0.006$) (Fig. 2C), suggesting that hypermethylation occurs on the *OCT2* promoter in RCC. In the sequenced CGI region, the fourth CpG site is located within a consensus sequence CACGTG called E-Box. Unlike the overall methylation, the E-Box site was exclusively hypermethylated in RCC tissues with stronger repression of OCT2 (Fig. 2D). The result was further confirmed by methylation-sensitive arbitrary qPCR (MS-AP-qPCR) assay. The performance of this assay was validated using control DNA templates (fig. S2, C and D). Methylation density at least 30% higher in tumor tissues than in adjacent nontumor tissues is defined as hypermethylation (*21*). As

shown in Fig. 2E, hypermethylation at the E-Box was observed in 15 of 25 RCC tissue samples with strong *OCT2* repression, but in none of those with weak repression. These results suggest that E-Box hypermethylation is associated with *OCT2* repression in RCC. However, we cannot discount the possibility that other CpG sites at the *OCT2* promoter region are also implicated in its transcriptional regulation.

Next, we examined whether DNA demethylation activates OCT2 expression in RCC cells. The *OCT2* promoter was hypermethylated in all three RCC lines (786-O, 769-P, and Caki-1) used in the study (Fig. 2F). Decitabine (DAC), a demethylating reagent that blocks cellular DNA methyltransferases (DNMTs), was used to globally inhibit DNA methylation in RCC cell lines. The effect of DAC on the demethylating *OCT2* promoter was monitored by analyzing E-Box methylation using MS-AP-qPCR (fig. S3). Upon treatment with DAC, *OCT2* transcription was activated in all three RCC cell lines in a dose-dependent manner (Fig. 2G). Western blot analysis confirmed that DNA demethylation by DAC induced OCT2 expression at the protein level in RCC cell lines (Fig. 2H). Together, we conclude that DNA hypermethylation represses OCT2 in RCC.

DNA hypermethylation inhibits MYC regulation of OCT2 in RCC

We next attempted to decipher how DNA methylation causes *OCT2* repression in RCC. The DNA methylation results described above revealed the association of E-Box hypermethylation with *OCT2* repression, which indicates a putative role of the E-Box in *OCT2* regulation. The E-Box within promoter CGIs is a preferential target site for MYC (*22*). MYC selectively binds to the E-Box and functions as a transcription factor to regulate gene expression. We identified MYC occupancy at *OCT2* proximal promoter in the normal kidney using a chromatin immunoprecipitation (ChIP) assay (Fig. 3A). To determine the role of MYC in regulating *OCT2*, we constructed 786-O cell lines that conditionally expressed short hairpin RNAs (shRNAs) specific to *MYC* (shMYC-15 and shMYC-17) or nontargeting shRNA (shNC). MYC was efficiently silenced in 786-O cells when shMYC expression was turned on in the presence of doxycycline (Dox) in the cell culture medium (Fig. 3B). DNA demethylation by DAC activated *OCT2* transcription in the absence of Dox and showed little effect on MYC expression. However, DAC failed to activate *OCT2* expression in MYC-depleted cells (Fig. 3C). These data suggest that MYC is a key factor involved in *OCT2* activation. To determine the importance of the E-Box in MYC-mediated regulation of *OCT2*, we introduced a site-specific mutation into the promoter construct. Luciferase assay showed that this E-Box mutation interfered with the ability of MYC to transactivate the *OCT2* promoter (Fig. 3D), indicating that MYC activates *OCT2* by interacting with the E-Box motif.

E-Box–mediated regulation is methylation-dependent (*23*–*25*). We therefore explored whether *OCT2* activation by MYC through the E-Box is controlled by DNA methylation. After in vitro methylation, the ability of MYC to transactivate the *OCT2* promoter was reduced to the basal level (Fig. 3E). ChIP assays further showed that DNA demethylation by DAC boosted MYC occupancy at the *OCT2* promoter in 786-O cells. The specificity of MYC antibody in ChIP assay was validated in cells expressing shRNA specific to MYC (Fig. 3F). These data suggest that MYC regulates *OCT2* transcription by occupying the unmethylated promoter. Overall, our results indicate that DNA hypermethylation in RCC inhibits MYC-mediated regulation of *OCT2* by preventing MYC occupancy at the E-Box motif of the *OCT2* promoter.

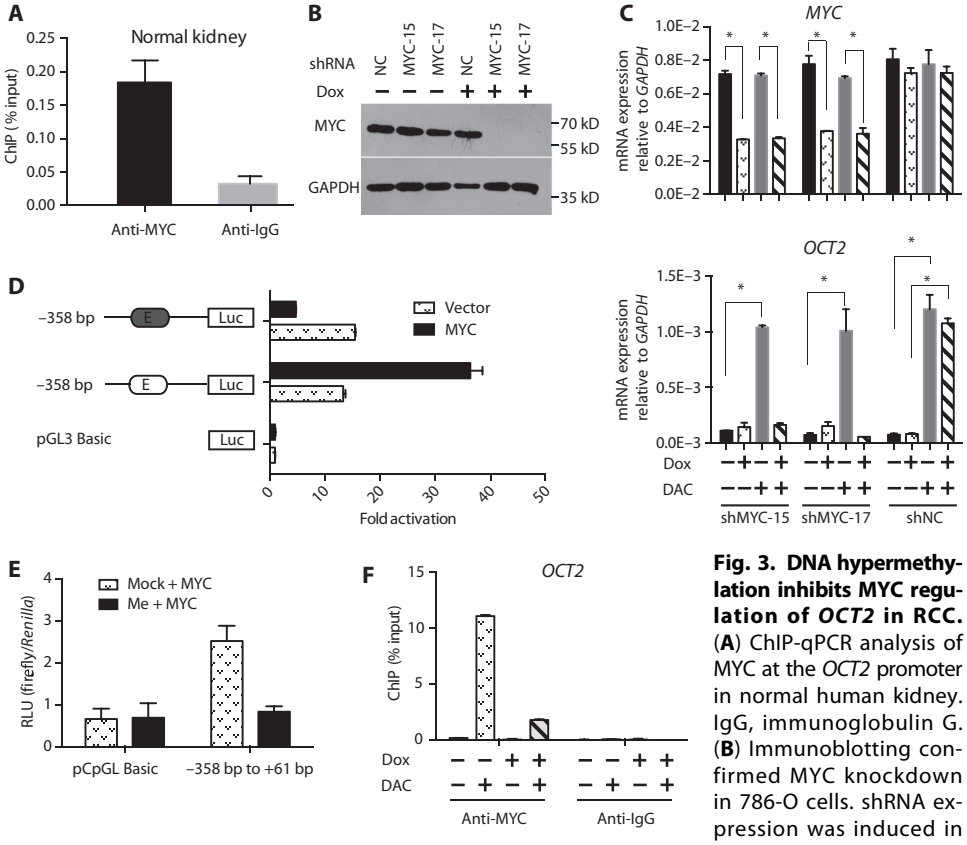

Fig. 3. DNA hypermethylation inhibits MYC regulation of *OCT2* in RCC. (**A**) ChIP-qPCR analysis of MYC at the *OCT2* promoter in normal human kidney. IgG, immunoglobulin G. (**B**) Immunoblotting confirmed MYC knockdown in 786-O cells. shRNA expression was induced in the presence of Dox (1 μg/ml) for 72 hours. (**C**) *MYC* (upper) and *OCT2* (bottom) mRNA expression in shRNA-expressing 786-O cells. Cells were treated with 2.5 μM DAC and/or Dox (1 μg/ml) for 72 hours [two-way analysis of variance (ANOVA) with Bonferroni's multiple comparison tests; * in top graph from left to right: $P < 0.0001$, $P < 0.0001$, $P = 0.0002$, and $P = 0.0004$; * in bottom graph from left to right: $P < 0.0001$, $P < 0.0001$, $P < 0.0001$, and $P < 0.0001$]. (**D**) HEK293 cells were transfected with *OCT2* reporter plasmids along with either MYC or empty expression vector (vector). The wild-type E-Box element CACGTG (white) was mutated into CTGTAG (gray). Fold activation was calculated by dividing the RLU from *OCT2* reporter transfection by RLU from blank pGL3 Basic vector transfection. Luc, luciferase. (**E**) HEK293 cells were transfected with methylated (Me) or mock-methylated *OCT2* reporter plasmids along with MYC. (**F**) ChIP-qPCR analysis of MYC at the *OCT2* promoter in 786-O cells. Cells expressing shMYC-15 were treated with 2.5 μM DAC and/or Dox (1 μg/ml) for 72 hours. Data are means ± SEM from technical triplicates in (A), biological triplicates with technical duplicates in (C) and (F), and biological triplicates in (D) and (E).

DNA hypermethylation inhibits MLL1 catalyzing H3K4 trimethylation at the OCT2 promoter

DNA hypermethylation usually coincides with the loss of trimethylated lysine 4 on histone H3 (H3K4me3) (*26*). H3K4me3 is an epigenetic mark of active chromatin state in most eukaryotes (*27*–*29*). By ChIP-qPCR analysis, highly enriched H3K4me3 was observed around the TSS of *OCT2* in normal kidneys and was reduced by 80% in paired RCC tumor with strong repression of *OCT2*. As a control, H3K4me3 enrichment at peptidylprolyl isomerase A (*PPIA*), which is stably expressed in renal normal and cancer tissues (*30*, *31*), was comparable between normal and paired tumor tissue (Fig. 4A), suggesting that gene-specific loss of H3K4me3 occurs at the *OCT2* promoter when *OCT2* is repressed in RCC.

To address the mechanism of H3K4me3 removal from the *OCT2* promoter in RCC, we first attempted to identify the "writer" responsible for adding H3K4me3 modification to the *OCT2* promoter. In mammals, at least six members of the COMPASS family of H3K4 methylases (including Set1A, Set1B, and MLL1 to MLL*4*) (*32*) trimethylate lysine 4 of H3. We assessed MLL1 occupancy at the *OCT2* promoter in the normal kidney (Fig. 4B). Then, we constructed 786-O cells that stably expressed shRNAs specific to MLL1 (shMLL1-03 and shMLL1-04) and nontargeting shRNA (shNC). As shown in Fig. 4C, MLL1 was successfully depleted from 786-O cells with the expression of specific shRNAs. DAC treatment activated *OCT2* transcription in nontargeting shRNA–expressing cells and showed little effect on MLL1 expression. Similar to MYC, when MLL1 was depleted from 786-O cells, DAC lost the ability to activate *OCT2* (Fig. 4D), suggesting that MLL1 is another crucial factor for *OCT2* regulation.

To further determine the role of MLL1 in regulating *OCT2*, we performed luciferase assays by cotransfecting *OCT2* promoter constructs with full-length or truncated MLL1 with SET [Su(var)3-9, Enhancer of zeste, Trithorax] domain deleted (MLL1-ΔSET). SET domain is the catalytic center of methyltransferase activity. Therefore, MLL1-ΔSET would lack the ability to catalyze H3K4me3 in the chromatin. The results showed that MLL1 activated the *OCT2* promoter and that this activity was dependent on the presence of SET domain (Fig. 4E), which suggested that MLL1 activates *OCT2* transcription by catalyzing H3K4me3 at the *OCT2* promoter. MLL1 protein also contains a CXXC domain, which selectively binds to unmethylated CpG (*33*). We found that DNA methylation in vitro completely blocked MLL1 transactivation of the *OCT2* promoter (Fig. 4F), indicating that *OCT2* regulation by MLL1 is controlled by DNA methylation. Next, ChIP results showed that H3K4me3 was absent at the *OCT2* promoter in 786-O cells. After DAC treatment, the occupancy was highly enriched in nontargeting shRNA–expressing 786-O cells but not in MLL1-silenced cells (Fig. 4G). *PPIA*, which is highly expressed in 786-O cells, was used as a control, and its expression was not affected by MLL1 knockdown (fig. S4). H3K4me3 enrichment at *PPIA*

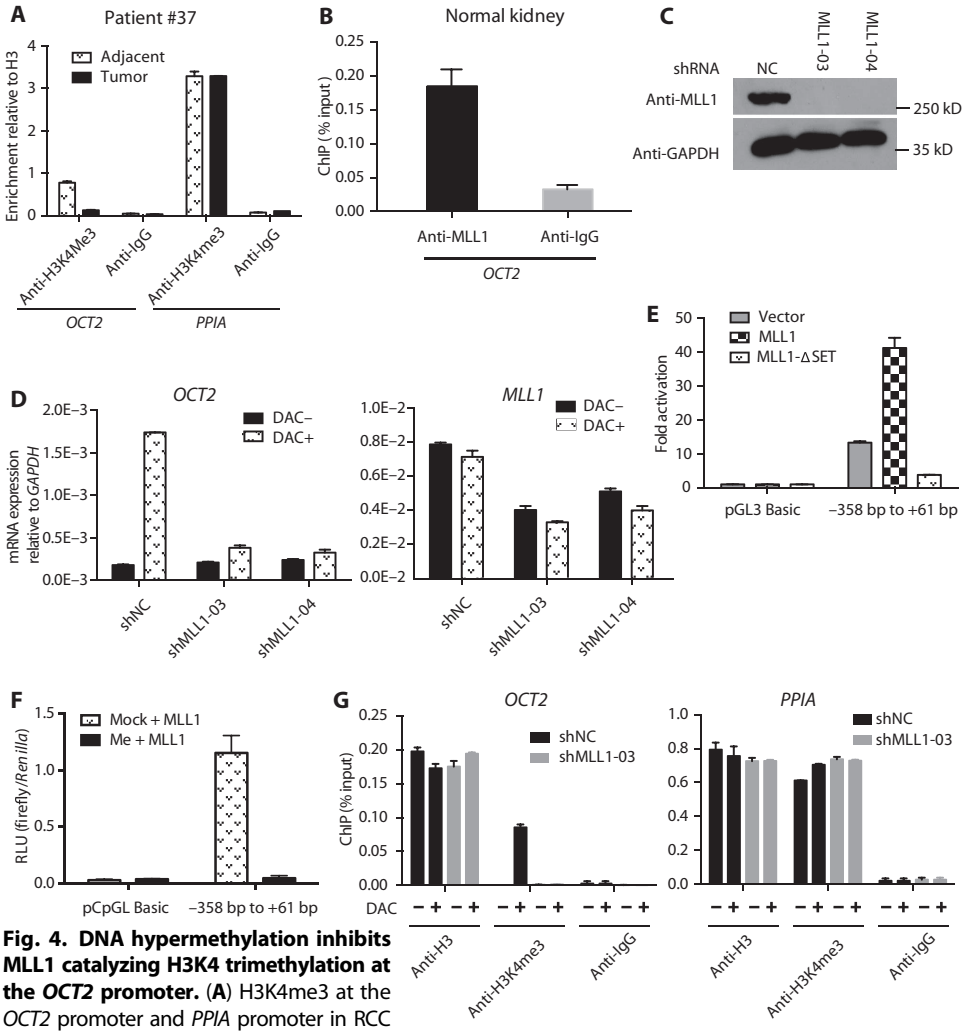

Fig. 4. DNA hypermethylation inhibits MLL1 catalyzing H3K4 trimethylation at the *OCT2* promoter. (**A**) H3K4me3 at the *OCT2* promoter and *PPIA* promoter in RCC tissues. ChIP with anti-H3, anti-H3K4me3, and anti-IgG was performed. Enrichments of anti-H3K4me3 and anti-IgG were normalized to that of anti-H3. (**B**) ChIP-qPCR analysis of MLL1 at the *OCT2* promoter in normal human kidney. (**C**) Immunoblotting confirmed MLL1 knockdown by shRNAs in 786-O cells. (**D**) mRNA expression of *OCT2* and *MLL1* in shRNA-expressing 786-O cells. Cells were treated with 2.5 μM DAC for 72 hours. (**E**) HEK293 cells were transfected with *OCT2* reporter plasmids along with MLL1, MLL1-ΔSET, or empty expression vector (vector). Fold activation was calculated by dividing the RLU from *OCT2* reporter transfection by RLU from blank pGL3 Basic vector transfection. (**F**) HEK293 cells were transfected with methylated (Me) or mock-methylated *OCT2* reporter plasmids along with MLL1. (**G**) ChIP-qPCR analysis showing the effect of MLL1 knockdown on H3K4me3 enrichment at *OCT2* and *PPIA* promoters in 786-O cells. Cells expressing shMLL1-03 or nontargeting shRNA (shNC) were treated with 2.5 μM DAC for 72 hours. Data are means ± SEM from technical triplicates in (A) and (B), biological triplicates in (E) and (F), and biological triplicates with technical duplicates in (D) and (G).

showed little response to DAC treatment and MLL1 knockdown (Fig. 4G). These results together provide evidence that both "writer" (MLL1) and "canvas" (unmethylated promoter) are prerequisites for catalyzing H3K4me3 modification at *OCT2*.

DNA methylation interferes with MYC recruitment of MLL1 to the OCT2 promoter

Luciferase assay results showed that MLL1 transactivation of the *OCT2* promoter depends on the E-Box sequence (Fig. 5A) and MYC expression (Fig. 5B), which indicates a crucial role of MYC in MLL1 regulation of *OCT2*. Next, we probed whether MLL1 catalyzing H3K4me3 at the *OCT2* promoter is MYC-dependent. ChIP analysis revealed that the expression of MYC shRNA disrupted the occupancy of MLL1 at the demethylated *OCT2* promoter (Fig. 5C). DAC treatment failed to induce H3K4me3 enrichment at the *OCT2* promoter in MYC-depleted cells. As a control, neither DAC treatment nor MYC knockdown showed any effect on H3K4me3 signature on *GAPDH* (Fig. 5D). Immunoprecipitation analysis further revealed a direct interaction between MYC and MLL1 in DAC-treated 786-O cells instead of untreated cells (Fig. 5E). On the basis of these results, we conclude that interaction with MYC is required for MLL1 recruitment to facilitate catalyzing H3K4me3 at the unmethylated *OCT2* promoter. Given that the occupancy of MYC at the *OCT2* promoter is controlled by DNA methylation, the data put together suggest a mechanism where DNA hypermethylation in RCC blocks MYC binding and interferes with MLL1 recruitment, which is required to catalyze H3K4me3 at the *OCT2* promoter, which finally represses *OCT2* transcription.

OCT2 activation by DAC sensitizes RCC cells to oxaliplatin

Oxaliplatin, a platinum-based chemotherapeutic agent, is mainly transported into cells by OCT2. Stable expression of OCT2 increased cellular accumulation (by 242%) and DNA adduct formation (by 229%) of oxaliplatin in 786-O cells (fig. S5, A and B). Accordingly, cells stably expressing OCT2 were 10 times more sensitive to oxaliplatin than the control cells [median inhibitory concentration (IC_{50}) values dropped from 51.3 to 4.62 μM] (fig. S5C).

On the basis of the central role of DNA methylation in OCT2 repression in RCC, we examined whether epigenetic activation of OCT2 by DAC sensitizes RCC cells to oxaliplatin. As shown in Fig. 6 (A and B), DAC treatment increased cellular accumulation (by 93, 59, and 66% in 769-P, 786-O, and Caki-1 cells, respectively) and DNA adduct formation (by 153, 135, and 88% in 769-P, 786-O, and Caki-1 cells, respectively) of oxaliplatin in all three RCC cell lines. Evaluated by the Chou-Talalay method, the sequential combination of DAC and oxaliplatin resulted in synergetic cytotoxicity, with combination index consistently below 0.8 in all three RCC cell lines tested (Fig. 6C). DAC pretreatment increased oxaliplatin sensitivity to 13, 6, and 4 times in 769-P, 786-O, and Caki-1 cell lines, respectively (Fig. 6D). By contrast, we found that combination with DAC did not sensitize RCC cells to cisplatin and carboplatin (fig. S6), which are also platinum-based chemotherapy drugs, but not favorable substrates of OCT2 (*6*). This result suggests the indispensable role of OCT2 in the synergistic effect observed in DAC and oxaliplatin combination therapy.

To further determine whether the synergistic effect depends on OCT2 activation, we assessed the efficacy of combination therapy in RCC cell lines expressing OCT2 shRNA. OCT2 expression was not activated by DAC treatment in the presence of OCT2 shRNA expression (Fig. 6E). Accordingly, neither increased cellular accumulation nor DNA adduct formation of oxaliplatin was observed after *OCT2* knockdown (Fig. 6, F and G). Drug combination analysis further showed that OCT2 shRNA expression markedly

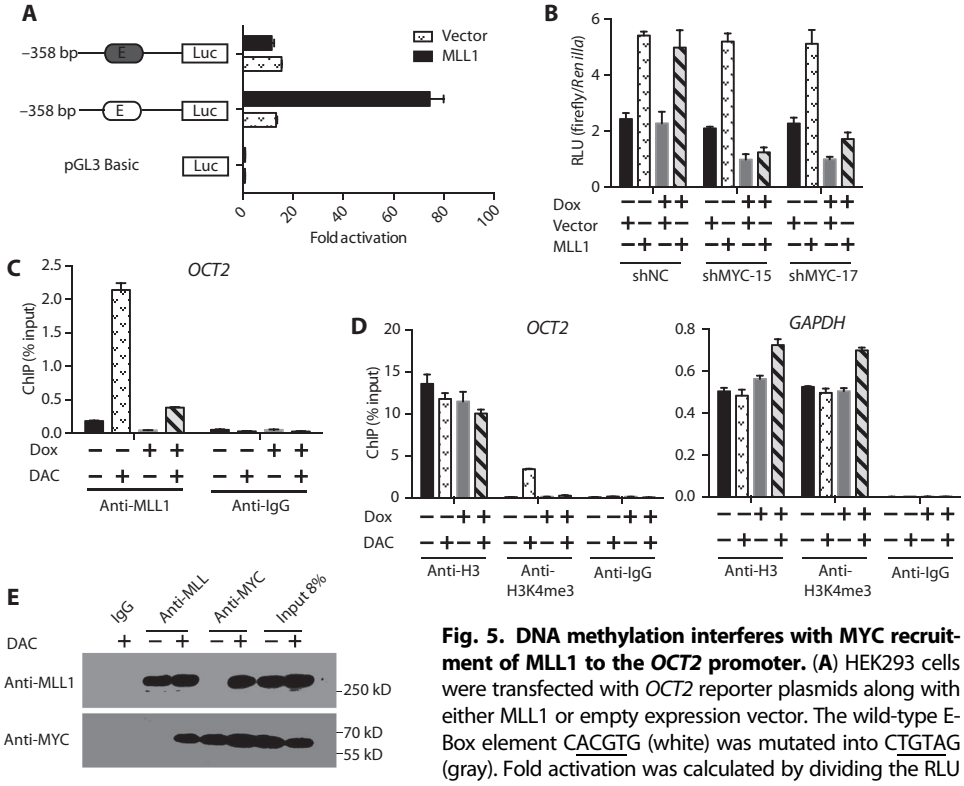

Fig. 5. DNA methylation interferes with MYC recruitment of MLL1 to the *OCT2* promoter. (**A**) HEK293 cells were transfected with *OCT2* reporter plasmids along with either MLL1 or empty expression vector. The wild-type E-Box element CACGTG (white) was mutated into CTGTAG (gray). Fold activation was calculated by dividing the RLU from *OCT2* reporter transfection by RLU from blank pGL3 Basic vector transfection. (**B**) Luciferase assay in 786-O cells expressing MYC shRNAs or nontargeting shRNA (shNC). Dox was added to the medium to induce shRNA expression. Cells were cotransfected with *OCT2* reporter plasmids along with either MLL1 or empty expression vector (vector). (**C**) ChIP-qPCR analysis shows the effect of DNA methylation and MYC expression on MLL1 occupancy at the *OCT2* promoter. (**D**) ChIP-qPCR analysis shows the effect of MYC knockdown on H3K4me3 enrichment at *OCT2* and *GAPDH* promoters. 786-O cells conditionally expressing shMYC-15 were used in (C) and (D). Cells were treated with 2.5 μM DAC or Dox (1 μg/ml) for 72 hours. (**E**) Coimmunoprecipitation assay for MYC and MLL1. 786-O cells with or without DAC treatment were used. A total of 8% of the cell lysates that were used for pull-down served as immunoblotting control. Pull-down antibodies are labeled at the top. Immunoblotting was performed with antibodies against MLL1 (top) and MYC (bottom). Data are means ± SEM from biological triplicates in (A) and (B) and biological triplicates with technical duplicates in (D) and (G).

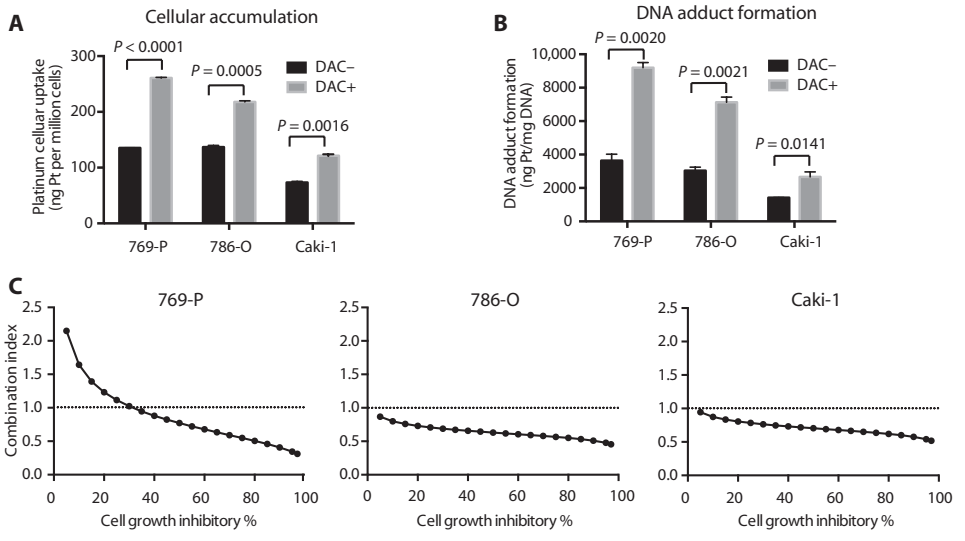

D

	IC_{50} of oxaliplatin (μM)		DRI of oxaliplatin
	Alone	Combo	
769-P	10.60	0.78	13
786-O	9.71	1.55	6
Caki-1	27.48	6.78	4
769-P–shNC	11.23	5.86	2
769-P–shOCT2-03	13.53	13.66	1
786-O–shNC	15.02	2.14	7
786-O–shOCT2-03	9.56	6.61	1
Caki-1–shNC	35.10	16.10	2
Caki-1–shOCT2-03	28.452	24.31	1

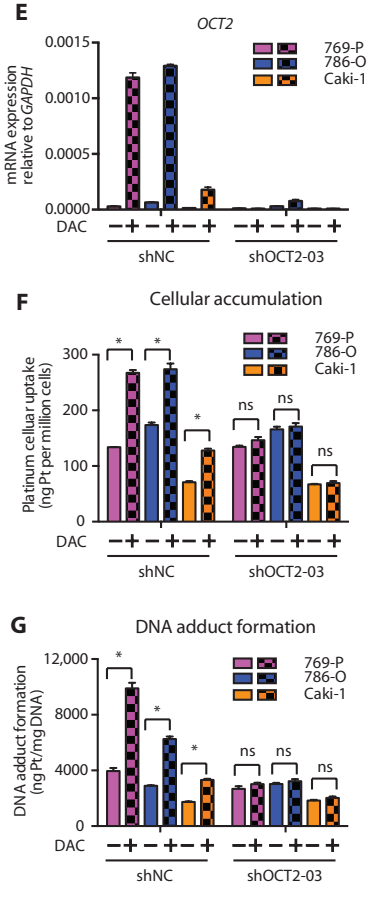

Fig. 6. DAC sensitizes RCC cells to oxaliplatin through OCT2 activation. (**A** and **B**) DAC treatment increased oxaliplatin cellular accumulation (A) and DNA adduct formation (B) in RCC cells (one-tailed unpaired *t* test). Cells were treated with 2.5 μM DAC for 72 hours and then exposed to 20 μM oxaliplatin for 4 hours. (**C**) Combination index–fraction affected plots of DAC and oxaliplatin combinations in RCC cells. Plots were generated using the CompuSyn software. Cytotoxicity index (CI) < 1, CI = 1, and CI > 1 indicate synergism, additive effect, and antagonism, respectively. Smaller CI value indicates stronger synergism. (**D**) IC_{50} values and dose reduction index (DRI) of oxaliplatin in RCC cells receiving oxaliplatin alone or combination treatment. DRI is the ratio of IC_{50} (alone) to IC_{50} (combo), which represents the fold-dose reduction of oxaliplatin at 50% inhibitory effect in combination. (**E**) Effects of *OCT2* knockdown on DAC-induced *OCT2* activation. (**F** and **G**) Effects of *OCT2* knockdown on oxaliplatin cellular accumulation (F) and DNA adduct formation (G) in RCC cell lines. RCC cell lines expressing *OCT2*-specific shRNA, shOCT2-03, and nontargeting shNC were used [two-way ANOVA with Bonferroni's multiple comparison tests; * in (F) from left to right: $P < 0.0001$, $P = 0.0010$, and $P = 0.0002$; * in (G) from left to right: $P = 0.0001$, $P < 0.0001$, and $P = 0.0002$; ns, not significant]. Data are means ± SEM from biological triplicates in (A), (B), (F), and (G) and biological triplicates with technical duplicates in (E).

inhibited RCC cells' sensitization to oxaliplatin by DAC pretreatment (Fig. 6D). Furthermore, MATE-2K, which exports oxaliplatin out of cells, was also repressed in RCC (fig. S7, A to C), and DAC pretreatment did not induce MATE-2K expression in RCC cell lines (fig. S7D). These results together suggest that DAC sensitizes RCC cell lines to oxaliplatin by activating OCT2-mediated uptake of oxaliplatin without boosting its efflux from RCC cells.

The enhanced effects of combination therapy with DAC and oxaliplatin were also demonstrated in 786-O and Caki-1 xenograft models. The drug administration timeline is shown in Fig. 7A. One week after DAC pretreatment, E-Box methylation at the *OCT2* promoter dropped to about 40% (fig. S8), and OCT2 expression was induced in xenografted tumors (fig. S9). At 24 hours after the first injection of oxaliplatin, tissue accumulation and DNA adduct formation of platinum in tumors receiving the combination treatment (Combo group) increased 2.6- and 2.8-fold, respectively, compared to those receiving oxaliplatin alone (Oxa group) (Fig. 7, C and D). This indicates that DAC pretreatment promotes the uptake of oxaliplatin into RCC cells in vivo. With regard to tumor growth, none of the single-agent treatments showed any discernible effect. By contrast, sequential combination of DAC and oxaliplatin not only remarkably delayed tumor growth but also resulted in >50% tumor shrinkage with prolonged treatment in the Caki-1 model (Fig. 7, E to G). Reversing the drug combination sequence by administering DAC 1 day after oxaliplatin proved ineffective in inhibiting tumor growth (Fig. 7, E and G). Collectively, these findings demonstrate that epigenetic activation of OCT2 by DAC promotes cellular accumulation of oxaliplatin and consequently sensitizes RCC cells to oxaliplatin both in vitro and in xenografts.

Despite the enhanced cytotoxicity to RCC cells, whether OCT2 activation by DAC can cause potential side effects to normal cells was a concern. Neuropathy is the most frequent adverse effect of oxaliplatin (*34*). Because production of reactive oxygen species is involved in oxaliplatin-induced neuropathy, we measured serum concentrations of advanced oxidized protein products (AOPPs) as a predictive marker of oxaliplatin-induced neuropathy

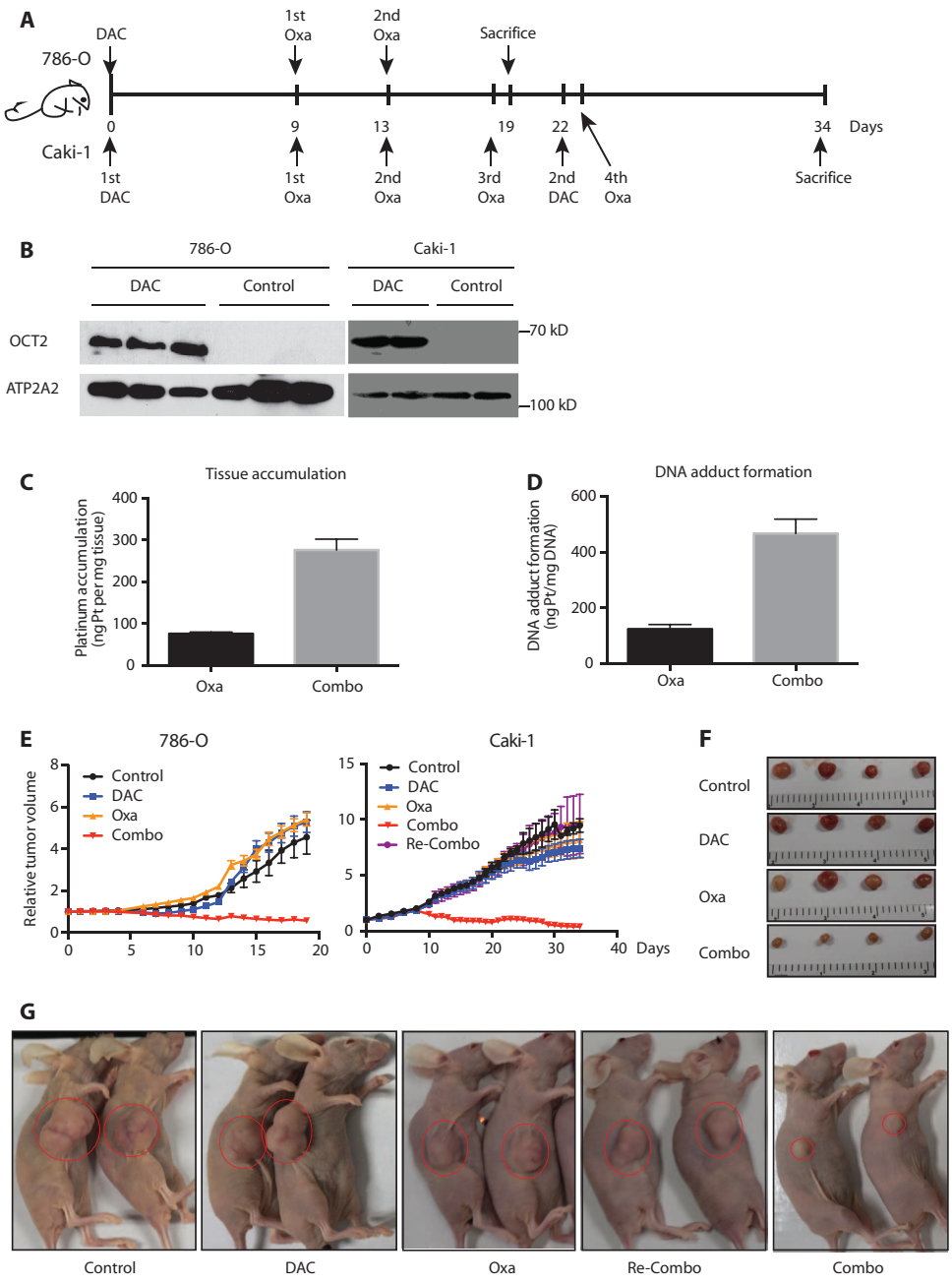

Fig. 7. DAC sensitizes RCC cells to oxaliplatin in xenograft models. (**A**) Experiment timeline and dosing schedule for xenograft models. (**B**) OCT2 induction in xenografted tumors. At 7 days after DAC treatment, crude membrane extracts were prepared from tumors to determine OCT2 expression. ATP2A2 was used as a loading control of membrane extracts. (**C** and **D**) Total platinum tissue accumulation and DNA adduct formation in 786-O xenografted tumors. At 24 hours after the first oxaliplatin administration, platinum concentration was determined by inductively coupled plasma mass spectrometry. Data are the means ± SEM from three mice. (**E**) Tumor growth curves in 786-O and Caki-1 xenograft models. Data are means ± SEM from five to six mice, except for the final stage of the Caki-1 model, when mice bearing oversized tumors were euthanized ahead of the end point. Data from individual mice are provided in table S6. Control, DAC, Oxa, and Combo indicate mice treated with saline, DAC alone, oxaliplatin alone, and DAC-oxaliplatin combination, respectively. Re-Combo indicates mice treated with the drug combination in the reverse sequence (DAC was administered 1 day after oxaliplatin). (**F**) Representative images of tumors after resection from 786-O xenografts at day 20. (**G**) Representative images of mice bearing Caki-1 xenografts at day 34.

(*35*). Mice treated with oxaliplatin alone or combination treatment all displayed an elevation of serum AOPP. However, we detected no significant difference between these groups of animals (fig. S10), which predicts a low risk of aggravated neuropathy in combination treatment. Next, to evaluate the cytotoxicity to normal renal and hepatic cells, we performed histological analysis on kidney and liver sections collected from Caki-1 xenografts. We found that DAC treatment has no discernable effect on OCT2 expression in normal kidney (fig. S11A), and nephrotoxicity was not observed in mice receiving treatment with oxaliplatin alone or in combination (fig. S11B). Unlike in the kidney, DAC treatment did induce OCT2 expression in liver (fig. S11A). However, no clear signs of increased toxicity to liver were observed in mice with combination treatment (fig. S11B).

DISCUSSION

Cancer cells defend themselves from chemotherapies with resistance-mediating transporters. So far, intensive studies have focused on the overexpression of drug exporters, including adenosine triphosphate (ATP)–binding cassette (ABC) and multidrug resistance protein (MRP) superfamilies, which actively pump drugs out of cells. Here, we suggest a correlation between the loss of uptake transporter expression and tumor cell resistance. Uptake transporters expressed in kidney proximal tubules include organic cation transporters (OCT2, OCT3, OCTN1, and OCTN2), organic anion transporters (OAT1, OAT2, OAT3, and OATP4C1), and peptide transporters (PEPT1 and PEPT2) (*36*). We analyzed data from the Oncomine cancer transcriptome database and found that most of these uptake transporters, except for OCTN2 and PEPT1, are transcriptionally repressed in RCC at varying degrees (*11*). Although most of the proteins showing reduced expression have yet to be characterized, previous studies strongly suggest that reduction of uptake transporters at least partially contributes to multidrug resistance in RCC. OCT3 expression in RCC cell lines has been shown to increase chemosensitivity to cytostatics transported by OCT3 (*37*). Here, we validated OCT2 repression at both transcription and protein

levels in RCC. Most of the samples were collected from patients with RCC at less-advanced tumor-node-metastasis stages, indicating that OCT2 repression already occurs during early stages of RCC oncogenesis. Future studies in renal cancer stem cells should help further decipher the role of OCT2 repression in RCC progression.

Figure S12 is a cartoon model illustrating the mechanisms underlying OCT2 repression in RCC. Our data show that the active *OCT2* promoter in the normal kidney is characterized by a hypomethylated CGI and H3K4 trimethylation. We also identified MLL1 as the H3K4 methyltransferase responsible for H3K4 trimethylation at the *OCT2* promoter. In particular, MLL1 binding at the *OCT2* promoter depends on the interaction with MYC. MYC binds to the unmethylated E-Box and recruits MLL1 to catalyze H3K4 trimethylation at the hypomethylated *OCT2* promoter. Binding of transcription factors and recruitment of H3K4 methyltransferases protect the CGI from methylation (*38*). In contrast, the repressive *OCT2* promoter in RCC is characterized by a hypermethylated CGI and the absence of H3K4 methylation. DNA hypermethylation tested at the E-Box prevents MYC binding, disrupts the interaction with MLL1, and further interferes with MLL1 catalyzing H3K4me3 at the *OCT2* promoter. In the absence of the active chromatin marker H3K4me3, *OCT2* transcription is inhibited. When the methylated CpGs are removed by DNA demethylating agents such as DAC, the MYC- and MLL1-mediated machinery is reestablished, thus reactivating *OCT2* transcription. The next question that remains is regarding the causality between DNA hypermethylation and H3K4 demethylation at the *OCT2* promoter during RCC tumorigenesis. DNA methylation is established by de novo DNMTs (DNMT3A and DNMT3B) and is perpetuated through cell division by maintenance DNMT (DNMT1) (*39*). The ADD domain in de novo DNMTs specifically recognizes unmethylated H3K4 (*39*–*42*). Thus, the removal of H3K4 methylation by histone lysine–specific demethylases is a prerequisite for establishing DNA methylation at *OCT2*.

Here, we elucidated part of the interactome that regulates OCT2 repression in RCC. However, some issues remain unclear: the specific DNMTs, histone lysine demethylases, and other chromatin regulators that function at the *OCT2* promoter; the mechanism by which these chromatin modifiers are recruited to the *OCT2* promoter; and the possibility of other transcription factors being involved in *OCT2* regulation. To better understand the complete network of *OCT2* regulation in RCC, reverse ChIP, also known as proteomics of isolated chromatin segments (PICh), may be required in the future to characterize the protein complexes associated with the *OCT2* locus in vivo (*43*, *44*). We also noted that, in comparison to the complete loss of expression at the protein level, *OCT2* transcriptional repression occurred at varying degrees, suggesting the coexistence of other pathways such as posttranscriptional and/or posttranslational regulation of OCT2 repression in RCC.

Oxaliplatin, a platinum-based anticancer drug, covalently binds to DNA and forms DNA adducts, triggering various signal transduction pathways that contribute to cell death. Insufficient DNA binding would cause platinum resistance in cancer cells, and thus, cellular accumulation of the drug is a crucial determinant of oxaliplatin cytotoxicity (*5*). Transportation of oxaliplatin is mediated by organic cation transporters (mainly by OCT2 and weakly by OCT3) as well as a member of the multidrug and toxin extrusion family, MATE-2K (*45*). Expression of these transporters controls oxaliplatin accumulation and cytotoxicity in cells. Organic cation transporters expressed on the basolateral side of renal tubules, especially OCT2, which is 20 times more abundant than OCT3 (*36*), mediate the uptake of oxaliplatin from the circulation into tubule epithelial cells. Subsequently MATE-2K expressed on the apical side actively pumps oxaliplatin out of the cells and into the urine. This pump-in and pump-out system prevents accumulation of oxaliplatin in normal renal cells, which partially explains why oxaliplatin therapy is usually devoid of nephrotoxicity (*45*). In contrast to normal renal cells, both OCT2 and MATE-2K are repressed in RCC. Inadequate accumulation of oxaliplatin in RCC cells results in therapy failure. After DAC treatment, only the expression of OCT2, but not MATE-2K, is restored in RCC cells, resulting in high uptake but low efflux of oxaliplatin and consequently high accumulation and increased cytotoxicity of oxaliplatin in RCC cells. The different transportation patterns between normal renal cells and RCC cells (as illustrated in fig. S13) make DAC-oxaliplatin combination a potential therapy targeting RCC cells and devoid of toxicity to noncancerous adjacent renal cells.

OCT2 expression in the nervous system plays a vital role in oxaliplatin-induced neuropathy (*46*). Whether DAC treatment affects OCT2 expression in nervous system is as yet unknown. Although the serum concentration of AOPPs predicts a low risk of aggravated neuropathy in combination therapy, further histological analysis in the peripheral nervous system will be needed to evaluate the effect of combination treatment on oxaliplatin-induced neurotoxicity.

In summary, our data suggest that sequential combination of DAC and oxaliplatin is a promising treatment option that sensitizes RCC cells to oxaliplatin by activating OCT2-mediated transportation of oxaliplatin into cancer cells. To facilitate clinical application, developing a sensitive method to analyze *OCT2* promoter methylation in body fluids will help fine-tune the combination strategy (including dosage, intervals, or combining with a third agent) and optimize the safety and efficacy of DAC-oxaliplatin combination therapy in the treatment of RCC.

To date, high-resolution and high-throughput technologies have provided unprecedented data regarding multidimensional cancer omics, including genome, epigenome, transcriptome, proteome, and metabolome systems (*47*). Our study highlights the potential of translating biological insights from the ever-increasing omics data into therapeutic advances.

MATERIALS AND METHODS

Study design

Driven by preliminary data from a public omics database, this study aimed to explore the epigenetic mechanisms underlying the repression of the organic cation transporter OCT2 in RCC and its translational relevance for targeted therapies. Tissue samples from 46 patients with RCC were collected from the Specimen Bank of Zhejiang Cancer Hospital at Hangzhou, China, with the approval by the Institutional Review Board of Zhejiang Cancer Hospital. Patient information was provided in table S1. In vivo efficacy studies in xenograft models were performed according to institutional guidelines, with the approval of Zhejiang University Animal Care and Use Committee. All animals were randomly assigned to treatment groups. Mice were euthanized if tumor size reached 1500 mm^3, and otherwise, they were euthanized at the end of the study. Experimental replications were defined in each figure legend. All statistical analyses were verified by K. Chen (School of Public Health, Zhejiang University).

Tissue microarray

Human RCC TMA was purchased from Shanghai Outdo Biotech (OD-CT-UrKid03). The TMA contained 62 tumorous and matched adjacent

nontumorous cores from 31 cases, including 10, 11, and 11 cases for clear cell RCC, chromophobe RCC, and papillary RCC, respectively (table S2).

Experimental methods

Sequence information of shRNAs and primers is provided in tables S3 and S4, respectively. Detailed descriptions of experimental methods are provided in Supplementary Materials and Methods.

Statistical analysis

Meta-analysis of *OCT2* differential transcription between the normal kidney and RCC populations was performed on Oncomine with one-tailed unpaired *t* test. Other statistical analyses were performed using GraphPad Prism version 6.0. Two-tailed Fisher's exact test was used to evaluate the difference of staining results between RCC tissues and adjacent nontumor tissues. Two-tailed paired *t* test was used to analyze (i) *OCT2* transcription difference and (ii) overall methylation frequency difference between RCC tissues and paired adjacent nontumor tissues. Two-tailed unpaired *t* test was used to analyze E-Box methylation differences between *OCT2* strongly and weakly repressed populations. One-tailed unpaired *t* test was used to analyze the differences in platinum amount between cells with and without DAC treatment. Two-way ANOVA with Bonferroni's multiple comparison test ($\alpha = 0.05$) was used in analyzing (i) the interaction between shRNA expression and DAC treatment and their effects on gene expression and (ii) the interaction between shRNA expression and DAC treatment and their effects on platinum accumulation and DNA adduct formation in RCC cell lines. One-way ANOVA with Bonferroni's multiple comparison test ($\alpha = 0.05$) was used in analyzing AOPP serum concentration differences between treatment groups.

SUPPLEMENTARY MATERIALS

www.sciencetranslationalmedicine.org/cgi/content/full/8/348/348ra97/DC1
Materials and Methods
Fig. S1. OCT2 is repressed in RCC.
Fig. S2. BSP and MS-AP-qPCR were validated with control DNA template.
Fig. S3. DAC treatment demethylates the E-Box at the *OCT2* promoter in RCC cell lines.
Fig. S4. MLL1 knockdown and DAC treatment do not affect *PPIA* expression in 786-O cells.
Fig. S5. OCT2 contributes to transport and cytotoxicity of oxaliplatin in RCC cells.
Fig. S6. Combination with DAC does not sensitize RCC cell lines to cisplatin and carboplatin.
Fig. S7. DAC treatment does not restore MATE-2K expression in RCC.
Fig. S8. DAC demethylates the E-Box at the *OCT2* promoter in xenografts.
Fig. S9. DAC induces OCT2 expression in xenografted tumors.
Fig. S10. Combination treatment does not increase AOPP serum concentration in Caki-1 xenografts.
Fig. S11. Histological analysis was performed on kidney and liver sections collected from Caki-1 xenografts.
Fig. S12. Cartoon model illustrates *OCT2* transcription machinery in the kidney.
Fig. S13. Cartoon model illustrates oxaliplatin transportation in normal renal cells and RCC cells.
Table S1. Tissue specimen information.
Table S2. TMA information.
Table S3. shRNAs used in this study.
Table S4. Primers used in this study.
Table S5. Methylation analysis results of individual tissues (provided as an Excel file).
Table S6. Tumor xenograft data (provided as an Excel file).

REFERENCES AND NOTES

1. B. Ljungberg, N. C. Cowan, D. C. Hanbury, M. Hora, M. A. Kuczyk, A. S. Merseburger, J.-J. Patard, P. F. A. Mulders, I. C. Sinescu, EAU guidelines on renal cell carcinoma: The 2010 update. *Eur. Urol.* **58**, 398–406 (2010).
2. B. I. Rini, S. C. Campbell, B. Escudier, Renal cell carcinoma. *Lancet* **373**, 1119–1132 (2009).
3. M. Chaouche, A.-L. Pasturaud, D. Kamioner, M. Grandjean, J. Franiatte, J.-M. Tourani, Oxaliplatin, 5-fluorouracil, and folinic acid (Folfox) in patients with metastatic renal cell carcinoma: Results of a pilot study. *Am. J. Clin. Oncol.* **23**, 288–289 (2000).
4. C. Porta, M. Zimatore, I. Imarisio, A. Natalizi, A. Sartore-Bianchi, M. Danova, A. Riccardi, Gemcitabine and oxaliplatin in the treatment of patients with immunotherapy-resistant advanced renal cell carcinoma: Final results of a single-institution phase II study. *Cancer* **100**, 2132–2138 (2004).
5. L. Kelland, The resurgence of platinum-based cancer chemotherapy. *Nat. Rev. Cancer* **7**, 573–584 (2007).
6. H. Burger, A. Zoumaro-Djayoon, A. W. M. Boersma, J. Helleman, E. M. J. J. Berns, R. H. J. Mathijssen, W. J. Loos, E. A. C. Wiemer, Differential transport of platinum compounds by the human organic cation transporter hOCT2 (*hSLC22A2*). *Br. J. Pharmacol.* **159**, 898–908 (2010).
7. S. Zhang, K. S. Lovejoy, J. E. Shima, L. L. Lagpacan, Y. Shu, A. Lapuk, Y. Chen, T. Komori, J. W. Gray, X. Chen, S. J. Lippard, K. M. Giacomini, Organic cation transporters are determinants of oxaliplatin cytotoxicity. *Cancer Res.* **66**, 8847–8857 (2006).
8. A. Yonezawa, S. Masuda, S. Yokoo, T. Katsura, K.-i. Inui, Cisplatin and oxaliplatin, but not carboplatin and nedaplatin, are substrates for human organic cation transporters (SLC22A1–3 and multidrug and toxin extrusion family). *J. Pharmacol. Exp. Ther.* **319**, 879–886 (2006).
9. S. Tatsumi, H. Matsuoka, Y. Hashimoto, K. Hatta, K. Maeda, S. Kamoshida, Organic cation transporter 2 and tumor budding as independent prognostic factors in metastatic colorectal cancer patients treated with oxaliplatin-based chemotherapy. *Int. J. Clin. Exp. Pathol.* **7**, 204–212 (2014).
10. H. Motohashi, Y. Sakurai, H. Saito, S. Masuda, Y. Urakami, M. Goto, A. Fukatsu, O. Ogawa, K.-i. Inui, Gene expression levels and immunolocalization of organic ion transporters in the human kidney. *J. Am. Soc. Nephrol.* **13**, 866–874 (2002).
11. D. R. Rhodes, J. Yu, K. Shanker, N. Deshpande, R. Varambally, D. Ghosh, T. Barrette, A. Pandey, A. M. Chinnaiyan, ONCOMINE: A cancer microarray database and integrated data-mining platform. *Neoplasia* **6**, 1–6 (2004).
12. M. Uhlén, L. Fagerberg, B. M. Hallström, C. Lindskog, P. Oksvold, A. Mardinoglu, Å. Sivertsson, C. Kampf, E. Sjöstedt, A. Asplund, I. Olsson, K. Edlund, E. Lundberg, S. Navani, C. A.-K. Szigyarto, J. Odeberg, D. Djureinovic, J. O. Takanen, S. Hober, T. Alm, P.-H. Edqvist, H. Berling, H. Tegel, J. Mulder, J. Rockberg, P. Nilsson, J. M. Schwenk, M. Hamsten, K. von Feilitzen, M. Forsberg, L. Persson, F. Johansson, M. Zwahlen, G. von Heijne, J. Nielsen, F. Pontén, Tissue-based map of the human proteome. *Science* **347**, 1260419 (2015).
13. G. Samimi, K. Katano, A. K. Holzer, R. Safaei, S. B. Howell, Modulation of the cellular pharmacology of cisplatin and its analogs by the copper exporters ATP7A and ATP7B. *Mol. Pharmacol.* **66**, 25–32 (2004).
14. G. D. Hariani, E. J. Lam, T. Havener, P.-Y. Kwok, H. L. McLeod, M. J. Wagner, A. A. Motsinger-Reif, Application of next generation sequencing to CEPH cell lines to discover variants associated with FDA approved chemotherapeutics. *BMC Res. Notes* **7**, 360 (2014).
15. M. Yin, J. Yan, E. Martinez-Balibrea, F. Graziano, H.-J. Lenz, H.-J. Kim, J. Robert, S.-A. Im, W.-S. Wang, M.-C. Etienne-Grimaldi, Q. Wei, *ERCC1* and *ERCC2* polymorphisms predict clinical outcomes of oxaliplatin-based chemotherapies in gastric and colorectal cancer: A systemic review and meta-analysis. *Clin. Cancer Res.* **17**, 1632–1640 (2011).
16. T. Efferth, Resistance to targeted ABC transporters in cancer, in *Resistance to Targeted Anti-Cancer Therapeutics,* B. Bonavida, Ed. (Springer International Publishing, Cham, Switzerland, 2015), 300 pp.
17. M. Ivanov, M. Kacevska, M. Ingelman-Sundberg, Epigenomics and interindividual differences in drug response. *Clin. Pharmacol. Ther.* **92**, 727–736 (2012).
18. M. A. Dawson, T. Kouzarides, Cancer epigenetics: From mechanism to therapy. *Cell* **150**, 12–27 (2012).
19. M. Aoki, T. Terada, M. Kajiwara, K. Ogasawara, I. Ikai, O. Ogawa, T. Katsura, K.-i. Inui, Kidney-specific expression of human organic cation transporter 2 (OCT2/SLC22A2) is regulated by DNA methylation. *Am. J. Physiol. Renal Physiol.* **295**, F165–F170 (2008).
20. M. Klug, M. Rehli, Functional analysis of promoter CpG-methylation using a CpG-free luciferase reporter vector. *Epigenetics* **1**, 127–130 (2006).
21. M. Weber, I. Hellmann, M. B. Stadler, L. Ramos, S. Pääbo, M. Rebhan, D. Schübeler, Distribution, silencing potential and evolutionary impact of promoter DNA methylation in the human genome. *Nat. Genet.* **39**, 457–466 (2007).
22. P. C. Fernandez, S. R. Frank, L. Wang, M. Schroeder, S. Liu, J. Greene, A. Cocito, B. Amati, Genomic targets of the human c-Myc protein. *Genes Dev.* **17**, 1115–1129 (2003).
23. G. Perini, D. Diolaiti, A. Porro, G. Della Valle, In vivo transcriptional regulation of N-Myc target genes is controlled by E-box methylation. *Proc. Natl. Acad. Sci. U.S.A.* **102**, 12117–12122 (2005).
24. M. Swarnalatha, A. K. Singh, V. Kumar, The epigenetic control of E-box and Myc-dependent chromatin modifications regulate the licensing of lamin B2 origin during cell cycle. *Nucleic Acids Res.* **40**, 9021–9035 (2012).
25. G. C. Prendergast, D. Lawe, E. B. Ziff, Association of Myn, the murine homolog of max, with c-Myc stimulates methylation-sensitive DNA binding and ras cotransformation. *Cell* **65**, 395–407 (1991).

26. D. Balasubramanian, B. Akhtar-Zaidi, L. Song, C. F. Bartels, M. Veigl, L. Beard, L. Myeroff, K. Guda, J. Lutterbaugh, J. Willis, G. E. Crawford, S. D. Markowitz, P. C. Scacheri, H3K4me3 inversely correlates with DNA methylation at a large class of non-CpG-island-containing start sites. *Genome Med.* **4**, 47 (2012).
27. A. Pekowska, T. Benoukraf, J. Zacarias-Cabeza, M. Belhocine, F. Koch, H. Holota, J. Imbert, J.-C. Andrau, P. Ferrier, S. Spicuglia, H3K4 tri-methylation provides an epigenetic signature of active enhancers. *EMBO J.* **30**, 4198–4210 (2011).
28. T. Kouzarides, Histone methylation in transcriptional control. *Curr. Opin. Genet. Dev.* **12**, 198–209 (2002).
29. R. Schneider, A. J. Bannister, F. A. Myers, A. W. Thorne, C. Crane-Robinson, T. Kouzarides, Histone H3 lysine 4 methylation patterns in higher eukaryotic genes. *Nat. Cell Biol.* **6**, 73–77 (2004).
30. M. Jung, A. Ramankulov, J. Roigas, M. Johannsen, M. Ringsdorf, G. Kristiansen, K. Jung, In search of suitable reference genes for gene expression studies of human renal cell carcinoma by real-time PCR. *BMC Mol. Biol.* **8**, 47 (2007).
31. H. Bjerregaard, S. Pedersen, S. R. Kristensen, N. Marcussen, Reference genes for gene expression analysis by real-time reverse transcription polymerase chain reaction of renal cell carcinoma. *Diagn. Mol. Pathol.* **20**, 212–217 (2011).
32. P. Wang, C. Lin, E. R. Smith, H. Guo, B. W. Sanderson, M. Wu, M. Gogol, T. Alexander, C. Seidel, L. M. Wiedemann, K. Ge, R. Krumlauf, A. Shilatifard, Global analysis of H3K4 methylation defines MLL family member targets and points to a role for MLL1-mediated H3K4 methylation in the regulation of transcriptional initiation by RNA polymerase II. *Mol. Cell. Biol.* **29**, 6074–6085 (2009).
33. M. D. Allen, C. G. Grummitt, C. Hilcenko, S. Y. Min, L. M. Tonkin, C. M. Johnson, S. M. Freund, M. Bycroft, A. J. Warren, Solution structure of the nonmethyl-CpG-binding CXXC domain of the leukaemia-associated MLL histone methyltransferase. *EMBO J.* **25**, 4503–4512 (2006).
34. M. W. Saif, J. Reardon, Management of oxaliplatin-induced peripheral neuropathy. *Ther. Clin. Risk Manag.* **1**, 249–258 (2005).
35. R. Coriat, J. Alexandre, C. Nicco, L. Quinquis, E. Benoit, C. Chéreau, H. Lemaréchal, O. Mir, D. Borderie, J.-M. Tréluyer, B. Weill, J. Coste, F. Goldwasser, F. Batteux, Treatment of oxaliplatin-induced peripheral neuropathy by intravenous mangafodipir. *J. Clin. Invest.* **124**, 262–272 (2014).
36. K. M. Morrissey, C. C. Wen, S. J. Johns, L. Zhang, S.-M. Huang, K. M. Giacomini, The UCSF-FDA TransPortal: A public drug transporter database. *Clin. Pharmacol. Ther.* **92**, 545–546 (2012).
37. V. Shnitsar, R. Eckardt, S. Gupta, J. Grottker, G. A. Müller, H. Koepsell, G. Burckhardt, Y. Hagos, Expression of human organic cation transporter 3 in kidney carcinoma cell lines increases chemosensitivity to melphalan, irinotecan, and vincristine. *Cancer Res.* **69**, 1494–1501 (2009).
38. Z. D. Smith, A. Meissner, DNA methylation: Roles in mammalian development. *Nat. Rev. Genet.* **14**, 204–220 (2013).
39. J. Du, L. M. Johnson, S. E. Jacobsen, D. J. Patel, DNA methylation pathways and their crosstalk with histone methylation. *Nat. Rev. Mol. Cell Biol.* **16**, 519–532 (2015).
40. S. K. T. Ooi, C. Qiu, E. Bernstein, K. Li, D. Jia, Z. Yang, H. Erdjument-Bromage, P. Tempst, S.-P. Lin, C. D. Allis, X. Cheng, T. H. Bestor, DNMT3L connects unmethylated lysine 4 of histone H3 to de novo methylation of DNA. *Nature* **448**, 714–717 (2007).
41. H. Cedar, Y. Bergman, Linking DNA methylation and histone modification: Patterns and paradigms. *Nat. Rev. Genet.* **10**, 295–304 (2009).
42. D. Jia, R. Z. Jurkowska, X. Zhang, A. Jeltsch, X. Cheng, Structure of Dnmt3a bound to Dnmt3L suggests a model for de novo DNA methylation. *Nature* **449**, 248–251 (2007).
43. J. Déjardin, R. E. Kingston, Purification of proteins associated with specific genomic Loci. *Cell* **136**, 175–186 (2009).
44. G. Mittler, F. Butter, M. Mann, A SILAC-based DNA protein interaction screen that identifies candidate binding proteins to functional DNA elements. *Genome Res.* **19**, 284–293 (2009).
45. S. Yokoo, A. Yonezawa, S. Masuda, A. Fukatsu, T. Katsura, K.-I. Inui, Differential contribution of organic cation transporters, OCT2 and MATE1, in platinum agent-induced nephrotoxicity. *Biochem. Pharmacol.* **74**, 477–487 (2007).
46. J. A. Sprowl, G. Ciarimboli, C. S. Lancaster, H. Giovinazzo, A. A. Gibson, G. Du, L. J. Janke, G. Cavaletti, A. F. Shields, A. Sparreboom, Oxaliplatin-induced neurotoxicity is dependent on the organic cation transporter OCT2. *Proc. Natl. Acad. Sci. U.S.A.* **110**, 11199–11204 (2013).
47. E. A. Vucic, K. L. Thu, K. Robison, L. A. Rybaczyk, R. Chari, C. E. Alvarez, W. L. Lam, Translating cancer 'omics' to improved outcomes. *Genome Res.* **22**, 188–195 (2012).
48. R. Beroukhim, J.-P. Brunet, A. Di Napoli, K. D. Mertz, A. Seeley, M. M. Pires, D. Linhart, R. A. Worrell, H. Moch, M. A. Rubin, W. R. Sellers, M. Meyerson, W. M. Linehan, W. G. Kaelin Jr., S. Signoretti, Patterns of gene expression and copy-number alterations in von-Hippel Lindau disease-associated and sporadic clear cell carcinoma of the kidney. *Cancer Res.* **69**, 4674–4681 (2009).
49. M. E. Lenburg, L. S. Liou, N. P. Gerry, G. M. Frampton, H. T. Cohen, M. F. Christman, Previously unidentified changes in renal cell carcinoma gene expression identified by parametric analysis of microarray data. *BMC Cancer* **3**, 31 (2003).
50. J. Jones, H. Otu, D. Spentzos, S. Kolia, M. Inan, W. D. Beecken, C. Fellbaum, X. Gu, M. Joseph, A. J. Pantuck, D. Jonas, T. A. Libermann, Gene signatures of progression and metastasis in renal cell cancer. *Clin. Cancer Res.* **11**, 5730–5739 (2005).
51. M. V. Yusenko, R. P. Kuiper, T. Boethe, B. Ljungberg, A. G. van Kessel, G. Kovacs, High-resolution DNA copy number and gene expression analyses distinguish chromophobe renal cell carcinomas and renal oncocytomas. *BMC Cancer* **9**, 152 (2009).

Acknowledgments: We appreciate P. Luo, J. Dai, and K. Zeng (Zhejiang University) for their help in establishing xenograft model. We thank J. Hess (University of Michigan) for providing MLL1-PCXN2 and MLL1-ΔSET-PCXN2 and M. Rehli (University Hospital Regensburg) for providing pCpGL luciferase vector. We thank K. Chen (Zhejiang University) for reviewing statistical analysis. We thank Y. Zhu (Zhejiang University) for histological evaluation. We also thank Y. Ma, S. Bai, and B. Cheng for critically reading the manuscript. **Funding:** This work was supported by grants from the National Natural Science Foundation of China (81573491), International Science and Technology Cooperation Program of China (2014DFE30050), the Fundamental Research Funds for the Central Universities of China Ministry of Education (2016XZZX001-08), and the Program for Zhejiang Leading Team of S&T Innovation (2011R50014). **Author contributions:** Conception and design: Y.L., S.Z., and L.Y. Development of methodology: Y.L. and X.Z. Data acquisition: Y.L., X.Z., Q.Y., Q.Z., L.Y., H.W., F.T., and H.J. Data analysis and interpretation: Y.L. Manuscript writing and editing: Y.L. Manuscript revision: S.Z. and X.Z. Study supervision: S.Z. and L.Y. **Competing interests:** The authors declare that they have no competing interests.

Submitted 24 January 2016
Accepted 21 June 2016
Published 20 July 2016
10.1126/scitranslmed.aaf3124

Citation: Y. Liu, X. Zheng, Q. Yu, H. Wang, F. Tan, Q. Zhu, L. Yuan, H. Jiang, L. Yu, S. Zeng, Epigenetic activation of the drug transporter OCT2 sensitizes renal cell carcinoma to oxaliplatin. *Sci. Transl. Med.* **8**, 348ra97 (2016).

Science Translational Medicine
AAAS

Epigenetic activation of the drug transporter OCT2 sensitizes renal cell carcinoma to oxaliplatin

Yanqing Liu, Xiaoli Zheng, Qinqin Yu, Hua Wang, Fuqing Tan, Qianying Zhu, Lingmin Yuan, Huidi Jiang, Lushan Yu and Su Zeng
(July 20, 2016)
Science Translational Medicine **8** (348), 348ra97. [doi: 10.1126/scitranslmed.aaf3124]

Editor's Summary

Opening a door into cancer cells

Renal cell carcinoma is a common cancer that is often resistant to chemotherapy. To address this, Liu *et al.* investigated the role of OCT2, a protein that normally transports oxaliplatin, a common chemotherapy drug, into cells. The authors found that OCT2 was epigenetically silenced in renal cancer and figured out the underlying mechanism, then designed a combination therapy with decitabine, a drug that reverses epigenetic silencing of OCT2, followed by oxaliplatin, and demonstrated its effectiveness in mouse models. The researchers also found that MATE-2K, another transporter that normally pumps oxaliplatin out of renal cells into the urine, is repressed in cancer cells regardless of decitabine treatment, so oxaliplatin accumulates in treated cancer cells, but not in the surrounding normal tissues.

Science Translational Medicine (print ISSN 1946-6234; online ISSN 1946-6242) is published weekly, except the last week in December, by the American Association for the Advancement of Science, 1200 New York Avenue, NW, Washington, DC 20005.